Computational Materials Science 127 (2017) 236–243

Quantitative Phase-Field Crystal Modeling of Solid-Liquid Interfaces for FCC Metals

Ebrahim Asadi [a,*] and Mohsen Asle Zaeem [b]

[a] *Department of Mechanical Engineering, The University of Memphis, Memphis, TN 38152, USA*
[b] *Department of Materials Science and Engineering, Missouri University of Science and Technology, Rolla, MO 65409, USA*

Abstract: This work deals with the quantification and application of the modified two-mode phase-field crystal model (M2PFC; Asadi and Asle Zaeem, Comput. Mater. Sci. 105 (2015) 110-113) for face-centered cubic (FCC) metals at their melting point. The connection of M2PFC model to the classical density functional theory is explained in this article. M2PFC model in its dimensionless form contains three parameters (two independent and one dependent) which are determined using an iterative procedure based on the molecular dynamics and experimental data. The quantification process and computer simulations are performed for Ni and Al as two case studies. The quantitative M2PFC models are used in series of numerical simulations to determine the two-phase FCC-liquid coexisting and the bulk properties at the melting points of Ni and Al. The calculated and predicted properties are the expansion in melting, elastic constants, solid-liquid interface free energy, and surface anisotropy, which are also compared with their available experimental or computational counterparts in the literature.

Keywords: Phase-field crystal; face-centered cubic; Ni; Al; solidification.

[*] Corresponding author; E-mail: easadi@memphis.edu (E. Asadi).

1. INTRODUCTION

Using computational materials science to predict micro- and nano- structural patterns has become more widespread amongst researchers mainly because of the recent advancements in high performance computing and the elevated cost of conducting experiments. Modeling and predicting structural patterns such as grain boundaries, dislocations, and defects in crystalline materials are of significant interest to materials scientists because these phenomena control the material properties. Therefore, design and engineering of structural patterns can possibly result in manufacturing of crystalline materials with improved properties.

Conventional atomistic scale models such as molecular dynamics (MD) are powerful methods to determine the structural patterns of materials at nano scale [1-5]. However, the phenomena such as solidification and grain growth, which control the structural patterns at their onset, essentially happen on diffusive time scales. On the other hand, most of the widely used mesoscale computational models for this purpose, such as phase-field models [6-8], do not provide atomistic resolution. Therefore, developing predictive atomistic models on diffusive time scales is a key component in accurately predicating the structural patterns in materials.

One of the recently developed atomistic models acting on diffusive time scales is the phase-field crystal (PFC) model [9-13]. PFC uses the crystal density field in its formulation as its order parameter. In PFC model, the crystal density field is constant in the liquid state and a periodic function in the crystalline state. Vacancy, dislocation, grain boundary, and two-phase solid-liquid interface formations as well as elasticity and plasticity are naturally incorporated in the PFC model. Consequently, PFC model can be used to calculate material properties such as solid-liquid interface free energy and surface anisotropy, grain boundary free energy, and elastic constants. Also, PFC can be used to quantitatively simulate problems such as solidification and grain growth in materials which basically happen on diffusive time scales. So far, PFC model has been used to simulate many phenomena in materials science including solidification [13-15], elastic deformation [16], spinoidal decomposition[17], grain-boundary premelting[18], and Kirkendall effect [19]. PFC model was also used to quantitatively simulate the two-phase solid-liquid coexistence of Fe by determining the PFC model parameters based on MD data [20-24]; the calculated results for solid-liquid interface free energy and surface anisotropy, elastic constants, and grain boundary free energy using PFC model were in reasonable agreements with the experimental data.

Some of the most technologically important materials such as Ni and Al have FCC crystal structures in the solid state. Therefore, it is important to extend the concept of a diffusive computational model such as PFC to fundamentally study and predict structural patterns of FCC materials. Wu et al. [24] presented a quantitative PFC model with FCC ordering by modifying the two-frequency Swift-Hohenberg (SH) equation [25] introduced by Lifshitz and Petrich [26]. Their model (two-mode PFC, or 2PFC) couples first two sets of crystal density waves corresponding to [111] and [200] density wave vectors. 2PFC model was recently modified (M2PFC) by the authors of this article [20, 27] to accurately minimize the free energy for the stable FCC or BCC crystals. Gao et al. [28] used 2PFC model to simulate nanoscale grain growth of FCC crystals. They simulated the grain growth, grain boundary with mismatch, and incoherent grain boundaries using the 2PFC model. In addition, 2PFC and M2PFC models can be used to simulate square lattice structures in two dimensions [27]. For instance, Adland et al. [29] used 2PFC model to study polycrystalline pattern evolution of square crystals. Wu et al. [24] provided a method to quantify their 2PFC model parameters based on some MD data such as liquid structure factor. They also calculated elastic constants and bulk modulus of Ni at its melting point. While they calculated reasonable C_{11} (112.5 GPa comparing to MD calculation of 155.4 GPa), their calculations of C_{12}, C_{44}, and bulk modulus significantly deviated from MD-calculated results. Nevertheless, quantitative PFC modeling of FCC-liquid structures has been done only for Ni, and also the capability of PFC models in predicting melting point properties such as expansion in melting, solid-liquid interface free energy and surface anisotropy have not been tested for any FCC material. To quantitatively validate the PFC modeling capabilities, it is necessary to calculatE these properties and directly compare them to their experimental counterparts. The outcomes of the comparisons can help quantifying the accuracy of PFC models in simulating solidification and grain growth problems for FCC crystals.

In this work, the connection between M2PFC model and the classical density functional theory (CDFT) is explained in details. Then, an iterative procedure is presented to determine the PFC model parameters for FCC materials at their melting point. As two case studies, the model parameters are calculated for Ni and Al based on available MD and experimental data, and the simulations and calculations are performed for these two materials. Bulk properties such as expansion in melting and elastic constants at the melting point are calculated. Also, the two-phase FCC-liquid coexisting problem is investigated using the quantified M2PFC model, and

properties such as FCC-liquid interface free energy and surface anisotropy are determined for Ni and Al. All the calculated properties are compared against their experimental or computational counterparts to test the accuracy of the quantitative M2PFC model.

2. Model Formulation

2.1. Connection to CDFT

The Helmholtz free energy in CDFT as suggested by Ramakrishnan and Yussouff [30] can be written as

$$\frac{F}{k_B T \rho_0} = \int d\boldsymbol{r} \left\{ [1+\mathrm{n}(\boldsymbol{r})] \ln[1+\mathrm{n}(\boldsymbol{r})] - \mathrm{n}(\boldsymbol{r}) \right\} - \frac{1}{2} \int d\boldsymbol{r} \int d\boldsymbol{r}' n(\boldsymbol{r}) \rho_0 c^{(2)}(|\boldsymbol{r}-\boldsymbol{r}'|)\, \mathrm{n}(\boldsymbol{r}'), \tag{1}$$

where k_B is the Boltzmann constant, T is the temperature, ρ_0 is the reference density, $n(\boldsymbol{r}) = (\rho(\boldsymbol{r}) - \rho_0)/\rho_0$ is the number density, and $c^{(2)}$ is the two-point correlation function. The first integral in Eq. (1) represents the ideal gas part of the free energy, and the second integral represents the excess free energy; the external free energy part is omitted. The logarithmic term in Eq. (1) can be approximated by a fourth-order polynomial as

$$[1+\mathrm{n}(\boldsymbol{r})] \ln[1+\mathrm{n}(\boldsymbol{r})] - \mathrm{n}(\boldsymbol{r}) \approx \frac{1}{2}\mathrm{n}(\boldsymbol{r})^2 - \frac{a}{6}\mathrm{n}(\boldsymbol{r})^3 + \frac{b}{12}\mathrm{n}(\boldsymbol{r})^4, \tag{2}$$

where a and b are fitting parameters [23]. We approximate the excess free energy by expanding the two-point correlation function in k space as

$$C(k) \approx C_0 + C_2 k^2 + C_4 k^4 + C_6 k^6 + C_8 k^8, \tag{3}$$

where $C(k) = \rho_0 c^{(2)}(k)$ and $C_0, C_2, C_4, C_6,$ and C_8 are constants. Substituting Eqs. (3) and (2) into Eq. (1) results in

$$\frac{F}{k_B T \rho_0} = \int d\boldsymbol{r} \left\{ \frac{1}{2}\mathrm{n}(\boldsymbol{r})[1 - C_0 + C_2\nabla^2 - C_4\nabla^4 + C_6\nabla^6 - C_8\nabla^8]\mathrm{n}(\boldsymbol{r}) - \frac{a}{6}\mathrm{n}(\boldsymbol{r})^3 + \frac{b}{12}\mathrm{n}(\boldsymbol{r})^4 \right\}. \tag{4}$$

If we assume

$$n = \frac{\phi}{\rho_0} + \frac{a}{2b}, \tag{5}$$

where ϕ is a function related to the number density. Substitute Eq. (5) into Eq. (4) results in

$$\frac{F}{k_B T \rho_0} = \int d\boldsymbol{r} \left\{ \frac{1}{2}\frac{\phi(\boldsymbol{r})}{\rho_0}[1 - C_0 - \frac{a^2}{4b} + C_2\nabla^2 - C_4\nabla^4 + C_6\nabla^6 - C_8\nabla^8]\frac{\phi(\boldsymbol{r})}{\rho_0} + \frac{b}{12}\frac{\phi(\boldsymbol{r})^4}{\rho_0^4} \right\}. \tag{6}$$

The free energy in Eq. (6) is identical to the free energy of the M2PFC model, which is [31]

$$F = \int_V f(\phi)\, d\mathbf{r}, \tag{7}$$

where

$$f = \frac{\phi(\mathbf{r})}{2}\left\{\alpha + \lambda[(q_0^2+\nabla^2)^2 + r_0][(q_1^2+\nabla^2)^2 + r_1]\right\}\phi(\mathbf{r}) + \frac{g}{4}\phi(\mathbf{r})^4, \tag{8}$$

with the following substitutions made in Eq. (6):

$$C_0 = 1 - \frac{a^2}{4b} - \frac{\rho_0}{k_B T}[\alpha + \lambda(\mathrm{r}_0 + \mathrm{q}_0^4)(\mathrm{r}_1 + \mathrm{q}_1^4)], \qquad C_2 = 2\frac{\rho_0 \lambda}{k_B T}[\mathrm{q}_1^2(\mathrm{r}_0 + \mathrm{q}_0^4) + \mathrm{q}_0^2(\mathrm{r}_1 + \mathrm{q}_1^4)],$$

$$C_4 = -\frac{\rho_0 \lambda}{k_B T}[(\mathrm{q}_0^2 + \mathrm{q}_1^2) + r_0 + r_1 + 2\,\mathrm{q}_0^2\mathrm{q}_1^2], \qquad C_6 = 2\frac{\rho_0 \lambda}{k_B T}(\mathrm{q}_0^2 + \mathrm{q}_1^2), \qquad C_8 = -\frac{\rho_0 \lambda}{k_B T},$$

$$b = \frac{3g\rho_0^3}{k_B T}, \qquad a^2 = 4b\{1 - C_0 - \frac{\rho_0}{k_B T}[\alpha + \lambda(\mathrm{r}_0 + \mathrm{q}_0^4)(\mathrm{r}_1 + \mathrm{q}_1^4)]\}. \tag{9}$$

The standard time-evolution equation for conserved fields is valid for ϕ as

$$\frac{\partial \phi(\mathbf{r})}{\partial t} = M\nabla^2 \frac{\delta F}{\delta \phi(\mathbf{r})}, \tag{10}$$

where M is the mobility constant. The dimensionless form of the M2PFC free energy may be also obtained from Eqs. (7), (8), and (10) as

$$F^* = \int_V f^*(\phi)\, d\boldsymbol{x}, \tag{11}$$

$$f^* = \frac{\psi(\boldsymbol{x})}{2}[-\varepsilon + [(1+\nabla^2)^2 + R_0][(Q_1^2+\nabla^2)^2 + R_1]]\psi(\boldsymbol{x}) + \frac{\psi(\boldsymbol{x})^4}{4}, \tag{12}$$

$$\frac{\partial \psi}{\partial t^*} = \nabla^2 \frac{\delta F^*}{\delta \psi}, \tag{13}$$

where ψ is the dimensionless density field and

$$\varepsilon = -\alpha / \lambda q_0^8, \qquad R_0 = r_0 / q_0^4, \qquad Q_1 = q_1 / q_0 \qquad R_1 = r_1 / q_0^4,$$

$$\psi = \phi\sqrt{g / \lambda q_0^8}, \quad \boldsymbol{x} = q_0\mathbf{r}, \qquad F^* = (g / \lambda^2 q_0^{13})F, \qquad t^* = tM\lambda q_0^7, \tag{14}$$

It is worth mentioning that Eqs. (11-13) are identical to those relations presented by Asadi and Asle Zaeem [20] for dimensionless form of M2PFC model showing that M2PFC model can be directly derived from CDFT.

2.2. Formulation for FCC-liquid

M2PFC model in its dimensionless form (Eqs. 11-13) have three model parameters, which are: ε, R_0, and R_1. In this section, we present some basic formulations of the model for FCC and liquid phases and explore the relations between the model parameters. The liquid free energy density is obtained by substituting the constant liquid density, ψ_l, in Eq. (12), integrating over a lattice cell, and dividing the resultant by the lattice volume as

$$f_l = -[\varepsilon - (1+R_0)(Q_1^4 + R_1)]\frac{\psi_l^2}{2} + \frac{\psi_l^4}{4}. \tag{15}$$

The dimensionless density field for FCC crystal including [111] and [200] density wave vectors ($Q_1 = \sqrt{4/3}$) is

$$\psi = \psi_s + 8A_s \cos qx \cos qy \cos qz + 2B_s(\cos 2qx + \cos 2qy + \cos 2qz), \tag{16}$$

where ψ_s is the average dimensionless FCC density, A_s and B_s are the density wave amplitudes for [111] and [200] density wave vectors, respectively, and $q = 1/\sqrt{3}$. The free energy density in the FCC phase is obtained by substituting Eq. (16) into Eq. (12), integrating over a lattice cell, and dividing the resultant by the lattice volume as

$$f_{fcc} = -[\varepsilon - (1+R_0)(\frac{16}{9} + R_1)]\frac{\psi_s^2}{2} + \frac{\psi_s^4}{4} + 4(\frac{1}{9}R_0 - \varepsilon + R_0R_1 + 3\psi_s^2)A_s^2$$

$$+3(3\psi_s^2 + R_0R_1 + \frac{1}{9}R_1 - \varepsilon)B_s^2 + 72A_s^2B_s\psi_s + 144A_s^2B_s^2 + 54A_s^4 + \frac{45}{2}B_s^4. \tag{17}$$

We previously showed that $R_0 = R_1(B_s^2 / A_s^2)$ in order to exactly minimize f_{fcc} at $q = 1/\sqrt{3}$ [20]. Minimizing f_{fcc} with respect to A_s and B_s results in two coupled equations as

$$[3\psi_s^2 - \varepsilon + R_0(\frac{1}{9} + R_1)]A_s + 18A_sB_s\psi_s + 36A_sB_s^2 + 27A_s^3 = 0,$$

$$[3\psi_s^2 - \varepsilon + R_1(\frac{1}{9} + R_0)]B_s + 12A_s^2\psi_s + 48A_s^2B_s + 15B_s^3 = 0. \tag{18}$$

Eqs. (18) should be numerically solved (for the given ε and R_1 parameters) to determine A_s and B_s. Furthermore, the coexisting solid and liquid densities (ψ_l and ψ_s, respectively) can be

determined using the standard common tangent line construction for the given ε and R_1 parameters.

In addition, the relations for the elastic constants can be obtained by applying isotropic, biaxial and simple shear deformations on the FCC lattice cell as

$$(x, y, x)_{isotropic} \to (x/(1+\xi), y/(1+\xi), z/(1+\xi)),$$

$$(x, y, x)_{biaxial} \to (x/(1+\xi), y/(1-\xi), z),$$

$$(x, y, x)_{shear} \to (x+\xi y, y, z), \tag{19}$$

where ξ is a small deformation. Comparing the free energy change due to the deformations in Eq. (19) to the corresponding elasticity relations leads to the following dimensionless elastic constants:

$$\tilde{C}_{11} = \frac{32}{9}[(\frac{1}{9}+R_1)A_s^2 + (\frac{4}{9}+4R_0+5R_1)B_s^2],$$

$$\tilde{C}_{12} = \tilde{C}_{44} = \frac{32}{9}[(\frac{1}{9}+R_1)A_s^2 + R_1 B_s^2]. \tag{20}$$

2.3. Model parameters determination

The liquid structure factor at the melting point for M2PFC model can be obtained by [31]

$$S(k) = \frac{k_B T_M}{\rho_l \lambda q_0^8 [-\varepsilon + 3\psi_l^2 + [(1-\tilde{k}^2)^2 + R_0][(4/3-\tilde{k}^2)^2 + R_1]}, \tag{21}$$

where $\tilde{k} = k/q_0$, ρ_l is the dimensional liquid density, and T_M is the melting point. Liquid structure factor can be also determined experimentally or using other computational methods such as MD simulations. For illustration, the experimental liquid structure factor for Ni and Al are shown by red dots in Fig. 1; they will be used as the target liquid structure factors in this study. The calculated structure factors at the melting point in the present model (Eq. 21) for $R_1 = -0.01$, $R_1 = 0$ and $R_1 = 0.01$ are also depicted in Fig. 1. The model parameters for determining the liquid structure factors from Eq. (21) are calculated using an iterative method which is explained in the following paragraphs. It is worthy to note that the liquid structure factor in the present model has a second peak located at $\sqrt{4/3}$ times of the location of the first peak. The height of the second peak is identical to the height of the first peak for $R_1 = 0$,

increases as R_1 decreases, and decreases as R_1 increases such that the second peak vanishes for sufficiently large R_1 parameters. The necessary relations to calculate all the PFC model parameters for different materials (except for g and R_1 parameters which will be discussed later) are determined by comparing the experimental liquid structure factor with the liquid structure factor relation at Eq. (21).

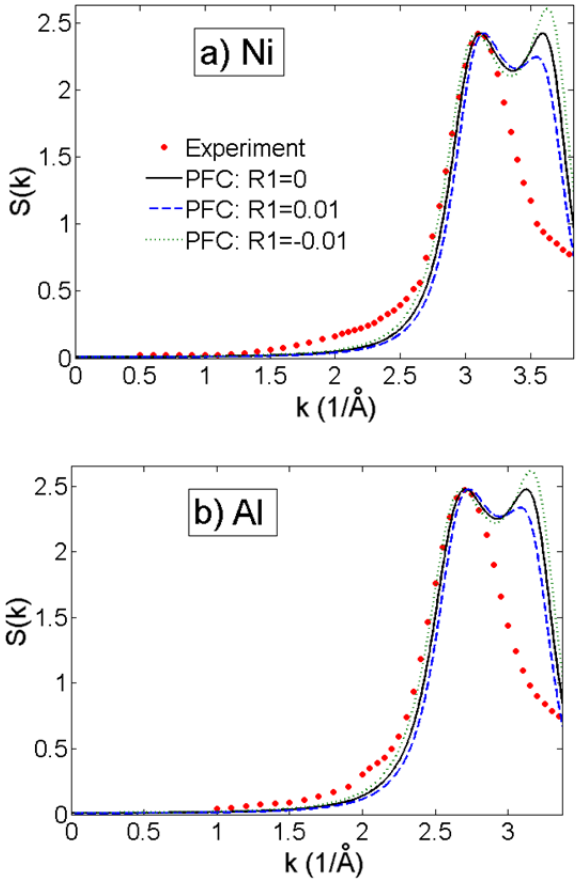

Fig. 1. Plot of the liquid structure factor at melting point in M2PFC model for $R_1 = -0.01$, $R_1 = 0$ and $R_1 = 0.01$ versus the experimental counterparts [32]: a) Ni; experiment performed at T= 1773 K, and b) Al; experiment performed at T= 943 K.

First, the location of the first peak of the structure factor in M2PFC model ($k_m = \tilde{k}_m q_0$) is determined by finding $\tilde{k}_m$ at which the first derivative of $S(k)$ is zero; q_0 is the location of the first peak of the experimental liquid structure factor. The resulting equation to determine $\tilde{k}_m$ is

$$(1-\tilde{k}_m^2)[(4/3-\tilde{k}_m^2)^2 + R_1] + (4/3-\tilde{k}_m^2)[(1-\tilde{k}_m^2)^2 + R_0] = 0. \quad (22)$$

This equation should be solved numerically for a given R_1 (R_0 is calculated as a function of R_1). Generally, $\tilde{k}_m \neq 1$ ($k_m \neq q_0$) unless $R_1 = 0$ which can be easily seen at Fig. 1. Also, increasing (decreasing) R_1 from zero shifts the location of the first peak to the bigger (smaller) k values. The second relation to determine the model parameters is obtained by equating the first peak of the liquid structure factor in the PFC model, $S(k_m)$, and that of the experiments, $S_{Exp}(q_0)$, as

$$\frac{k_B T_M}{\rho_l \lambda q_0^8 [-\varepsilon + 3\psi_l^2 + [(1-\tilde{k}_m^2)^2 + R_0][(4/3-\tilde{k}_m^2)^2 + R_1]} = S_{Exp}(q_0). \quad (23)$$

To obtain the third relation, the second derivative of the correlation function in the Fourier space ($C(k) = 1 - 1/S(k)$) needs to be determined at the location of the first peak, $C''(k_m) = S''(k_m)/S^2(k_m)$, and the calculated values utilizing the structure factors of the M2PFC model and experiments needs to be equated:

$$\frac{-8\lambda q_0^6 \rho_l}{k_B T_M} \tilde{k}_m^2 [4(4/3-\tilde{k}_m^2)(1-\tilde{k}_m^2) + (1-\tilde{k}_m^2)^2 + (4/3-\tilde{k}_m^2)^2 + R_0 + R_1] = C''_{Exp}(q_0). \quad (24)$$

Utilizing the relation $\varepsilon = -\alpha/\lambda q_0^8$ and Eqs. (23-24), we obtain

$$\lambda = \frac{-C''_{Exp}(q_0) k_B T_M}{8 q_0^6 \rho_l \tilde{k}_m^2 [4(4/3-\tilde{k}_m^2)(1-\tilde{k}_m^2) + (1-\tilde{k}_m^2)^2 + (4/3-\tilde{k}_m^2)^2 + R_0 + R_1]}, \quad (25)$$

$$\varepsilon = 3\psi_l^2 + [(1-\tilde{k}_m^2)^2 + R_0][(4/3-\tilde{k}_m^2)^2 + R_1] - \frac{k_B T_M}{\rho_l \lambda q_0^8 S_{Exp}(q_0)}. \quad (26)$$

Consequently, all the parameters in M2PFC model (except for g and R_1) are determined in terms of q_0, $S_{Exp}(q_0)$, $C''_{Exp}(q_0)$, ρ_l, ψ_l, and T_M using Eqs. (22, 25, 26). It is worth mentioning that ε cannot be explicitly calculated from Eq. (26) because ψ_l is a function of ε (through the

standard common tangent line construction). Thus, employing an iterative approach will be necessary to determine ε from Eq. (26) for a given R_1.

The relation for g is obtained by comparing the fluctuations of the solid density as

$$g_A = \frac{\lambda q_0^8 A_s^2}{\rho_l^2 u_{111}^2}, \quad g_B = \frac{\lambda q_0^8 B_s^2}{\rho_l^2 u_{200}^2}, \tag{27}$$

where u_{111} and u_{200} are the real solid density wave amplitudes related to [111] and [200] density wave vectors, respectively. Also, g_A and g_B denote the parameter g as calculated using the information for the first and second density wave amplitude, respectively. In order to determine u_{111} and u_{200}, we fit a Gaussian function to the fluctuations of atoms in the solid as calculated by the MD simulations explained in section II-F in Ref. [22]. Let's denote the standard deviation of the position of the atoms from their ideal location by u_r where u_r is averaged over all the atoms in the simulation box; Then, the real solid density wave amplitudes are calculated as $u_{111} = \exp(-q_0^2 \, u_r^2 / 2)$ and $u_{200} = \exp(-q_1^2 \, u_r^2 / 2)$. Ideally, g_A should be equal to g_B, and the role of R_1 parameter is to make g_B as close as possible to g_A by controlling A_s / B_s ratio; A_s and B_s are calculated through the standard common tangent line construction. In this work, for the sake of simplicity, we use the average of g_A and g_B equal to g. Therefore, all the parameters in the M2PFC model (except R_1) can be determined for specific materials by providing the liquid structure factor, liquid density, melting point, and standard deviation of the position of the atoms in the solid state. We still have the freedom of choosing R_1, and we will use it to produce the experimental elastic constants in the PFC model (explained in the next section) rather than fitting to another data point on the experimental liquid structure factor. For example, R_1 parameter may be used to lower the second peak of the liquid structure factor in the model or even making it to disappear (similar to the experiments; see Fig. 1). However, the amplitude of the second solid density wave vector (B_s) also decreases as R_1 increases such that for sufficiently big R_1 values (necessary to vanish the second peak of the liquid structure factor) the effect of the second density wave vector is negligible ($B_s \approx 0$) and M2PFC becomes identical to the one-mode PFC.

3. Case Studies: Ni and Al

3.1 Model parameters

The required input material properties to determine M2PFC model parameters for Ni and Al are listed at Table 1. The material properties q_0, $S_{Exp}(q_0)$, $C''_{Exp}(q_0)$, u_{111}, u_{200}, ρ_l, and T_M are obtained from experiments [32], and u_r is calculated using the modified embedded-atom method (MEAM) interatomic potentials develop by Asadi et al. [33] in MD simulations.

Table 1. The input material properties for M2PFC model for Ni and Al.

	q_0 (1/Å)	$S_{Exp}(q_0)$	$C''_{Exp}(q_0)$ (Å^2)	ρ_l (atom/Å^3)	T_M (K)	u_r (Å)
Ni	3.114	2.423	-6.426	0.0801	1728	0.1541
Al	2.706	2.476	-6.333	0.0530	934	0.1833

Following the iterative method which was discussed in details in section 2.3, M2PFC model parameters ε, ψ_l, ψ_s, A_s, B_s, and $\tilde{k}_m$, for a given R_1 parameter, can be determined using the data provided in Table 1. For instance, these PFC model parameters for five different R_1 values are calculated for Ni and listed in Table 2.

Table 2. The calculated Ni M2PFC model parameters for different value of R_1.

R_1	–0.02	–0.01	0	0.01	0.02
ε	0.016800	0.014899	0.013532	0.012878	0.013092
ψ_l	-0.093358	-0.086554	-0.080459	-0.075864	-0.073643
ψ_s	-0.092957	-0.086234	-0.080202	-0.075652	-0.073452
A_s	0.017491	0.016261	0.015178	0.014398	0.014078
B_s	0.013817	0.012736	0.011737	0.010938	0.010465
$\tilde{k}_m$	0.982028	0.990962	1	1.008706	1.016424

It is interesting to point out that $\tilde{k}_m$ increases as R_1 increases, and $\tilde{k}_m = 1$ for $R_1 = 0$. Also, both ψ_l and ψ_s decrease as R_1 increases. Furthermore, both A_s and B_s decrease by increasing R_1; while B_s constantly decreases toward zero, the decrement rate of A_s slows down for larger R_1 values. This behavior suggests that B_s vanishes for sufficiently large value of R_1 and M2PFC model becomes identical to one-mode PFC model.

In Table 3, C_{11} and C_{44} elastic constants ($C_{12} = C_{44}$) and the expansion in melting (ΔV) for Ni are reported for $R_1 = -0.02$, -0.01, 0, 0.01, and 0.02 using the corresponding model parameters listed in Table 2. The dimensional elastic constants are calculated using $C_{ij} = (\lambda^2 q_0^{16} / g)\tilde{C}_{ij}$ where $\tilde{C}_{ij}$ are the dimensionless elastic constants determined at Eqs. (20). The expansion in melting is calculated from the calculated dimensional solid and liquid densities. The relation between the dimensional and dimensionless densities can be readily obtained from Eq. (5) as

$$\rho = \rho_l + \psi\sqrt{\frac{\lambda q_0^8}{g}} + \frac{a\rho_l}{2b} \tag{28}$$

where a and b are defined in Eq. (9).

Table 3. The calculated elastic constants at melting point (C_{11} and C_{44}, in GPa) and expansion in melting (ΔV, Å^3/atom) for Ni using M2PFC model for $R_1 = -0.02, -0.01, 0, 0.01,$ and 0.02.

R_1	–0.02	–0.01	0	0.01	0.02
C_{11} [a]	90.96	127.17	173.37	228.08	282.06
C_{44} [a]	26.02	36.82	51.11	68.94	87.86
ΔV [b]	0.2725	0.2355	0.2042	0.1793	0.1670

[a] Embedded-atom method (EAM) MD calculations [24]: $C_{11} = 155.4,$ and $C_{44} = 66.0$.

[b] Experiment [33]: $\Delta V = 0.54$.

The data listed in Table 3 show that, as R_1 increases elastic constants increase while the expansion in melting decreases. Therefore, the variations of the elastic constants and expansion in melting with the variation of R_1 may be used as criteria to select R_1 (and consequently all the model parameters). First, it should be noted that the present model calculates the expansion in melting for the considered FCC crystals to be approximately half of its experimental value. Selecting bigger negative R_1 slightly increases the expansion in melting but significantly decreases the elastic constants. So, selecting negative R_1 values is favorable to improve the calculation of expansion in melting for Ni, but it cannot be used as the main selecting criterion. Looking at the elastic constant calculations for Ni reveals that the MD-calculated C_{11} is achieved by selecting a small negative R_1 while the MD-calculated C_{44} is obtained by selecting a small positive R_1. Since selecting a negative R_1 value also improves the calculation of the expansion in melting, we use fitting to the target C_{11} as our main criterion to select R_1. Consequently, the following procedure may be followed to systemically determine the optimized M2PFC model parameters with minimum errors for a given material: 1) select an R_1 parameter, 2) use the selected R_1 parameter in Eqs. (26-28) to determine ε by an iterative procedure (see section 2.3 for details), 3) use the calculated ε to determine ψ_l, ψ_s, A_s, B_s, and $R_0 = R_1(B_s^2 / A_s^2)$ parameters, 4) use all the calculated properties to determine C_{11} and compare it to the target value, and 5) update the R_1 parameter based on the outcome of the comparison in step 4, and repeat steps 2 to 5 until the desired accuracy is achieved.

The above-mentioned systematic procedure to determine M2PFC model parameters for solid-liquid coexistence of FCC materials at their melting point results in the selection of $R_1 = -0.004$ for Ni. It should be noted that the present PFC model in its current form results in a significant error in the calculation of C_{12} elastic constant because it calculates $C_{12} = C_{44}$; e.g. the MD-calculated C_{12} for Ni is 124.7 GPa. Table 4 lists all the selected M2PFC model parameters for Ni and Al. Since to the best knowledge of the authors, there are no reported elastic constants for Al at its melting point in the literature, we selected the same R_1 value for Al.

Table 4. The selected M2PFC model parameters for Ni and Al corresponding to $R_1 = -0.004$.

	ε	ψ_l	ψ_s	A_s	B_s	$\tilde{k}_m$
Ni	0.014003	-0.082765	-0.082488	0.015582	0.012118	0.996393
Al	0.018478	-0.094869	-0.094452	0.017896	0.013897	0.996404

In Table 5, we compare M2PFC-calculated elastic constants and expansion in melting (using the parameters reported in Table 4) with their available experimental or computational counterparts in the literature. It is clear that the present model can be used to produce the accurate C_{11} and C_{44} constants. Furthermore, the present model calculates the expansion in melting approximately half of its experimental value. The input material property $C''_{Exp}(q_0)$ is the parameter which is mostly controlling the expansion in melting and one may use bigger $C''_{Exp}(q_0)$ (and repeat the R_1 selection process) in order to improve the expansion in melting calculations. In this fitting procedure, the liquid density is always equal to its target value, and the only other factor affecting the expansion in melting is the solid density which can be calculated using Eq. (28), or $\Delta V = 1/\rho_l - 1/(\rho_l + \psi_s\sqrt{\lambda q_0^8/g} + \rho_l a/2b)$. In ΔV relation all the parameters are material properties except for $\psi_s\sqrt{\lambda/g}$ and a/b terms. $\psi_s\sqrt{\lambda/g}$ is a negative quantity and its absolute value decreases as $C''_{Exp}(q_0)$ increases (smaller absolute value since $C''_{Exp}(q_0)$ is negative). The a/b term is a positive quantity and its value decreases as $C''_{Exp}(q_0)$ increases but with a lower rate than the decrement rate of $\psi_s\sqrt{\lambda/g}$ term such that their competition results in higher expansion in melting. It is worth mentioning that the liquid isothermal compressibility, that has a direct relation to C_0, is influencing the calculation of the expansion in melting through the parameter a (see Eq. 9), as it was suggested in previous PFC works [23]; however, C_0 is not the only factor controlling the expansion in melting in the present PFC model. The error in calculating ΔV can be also explained by comparing the density profile of the PFC model to DFT results as it was done in Ref. [23]. The present PFC model results in broader peaks for FCC materials which results in overestimating temperature; thus, underestimating the expansion in melting. It is worth mentioning that DFT uses the full structure factor in its formulation while the present PFC model uses only two peaks of the structure factor in its formulations. One of these

peaks must be the first peak as it has the biggest height, but the choice of the second peak is arbitrary; i.e. we have used the first two peaks in the current formulation and parameter determination procedure. Therefore, it is possible to underestimate, overestimate, or recover the correct width of the density profile and contingently determine the expansion in melting by varrying the choice of the second peak; e.g. the present PFC model which was previously employed for BCC materials (Fe) results in calculating the correct expansion in melting by using the first two peaks in its formulation [34].

Table 5. Elastic constants (C_{11} and C_{44}) at melting point and expansion in melting (ΔV) for Ni, Cu, and Al calculated using M2PFC model and the parameters reported in Table 4.

	Ni			Al	
	present	PFC[a]	Exp./MD	present	Exp./MD
C_{11} (GPa)	153.7	112	155.4[b]	40.1	--
C_{12} (GPa)	44.9	33.1	124.7[b]	11.8	--
C_{44} (GPa)	44.9	33.1	66.0[b]	11.8	--
ΔV (Å^3/atom)	0.214	--	0.54[c]	0.418	1.14[c]

[a] Two-mode PFC model by Wu et al. [24].

[b] Embedded-atom method MD calculations [24].

[c] Experiments reported in [33].

3.2. FCC-liquid coexistence

The time-evolution equation of M2PFC model (Eq. 12) is of tenth order in spatial derivatives. In order to solve this tenth-order partial differential equation (PDE), four auxiliary functions (P, R, S, and T) are defined such that the tenth-order time-evolution PDE is reduced to the following system of five second-order PDEs:

$$\frac{\partial \psi}{\partial t} = \nabla^2\{[(1+R_0)(16/9+R_1)-\varepsilon]\psi + 2[R_1+R_0+28/9]P + [R_0+R_1+73/9]R + (14/3)T + S + \psi^3\},$$
$$P = \nabla^2\psi, \qquad R = \nabla^2 P, \qquad S = \nabla^2 R, \qquad T = \nabla^2 S. \tag{29}$$

Periodic boundary conditions are used in all directions and the model parameters listed in Table 4 are used for Ni and Al, accordingly. The FCC-liquid coexisting structures consisting of $m \times m \times n$ periodic lattice cells are constructed in order to determine FCC-liquid interface free energy and anisotropy for Ni and Al. The normal to the FCC-liquid interface plane (direction related to n) is either [100] or [110] direction. The value of n is typically much greater than m to minimize the pressure at the normal direction; e.g. $m = 2$ and $n = 70$ when [100] is the normal direction. Initially, the central half of the atoms are solid (Eq. 16) and the rest is liquid ($\psi = \psi_l$). Then, system of PDEs in Eq. (29) is solved for a sufficiently long time until the total free energy of the system remains constant and a two-phase FCC-liquid structure is achieved. In the concept of finite element method, cubic elements with implicit adaptive time stepping and backward-Euler method is used to solve the system of PDEs in Eq. (29). For all the simulations, the length of the cubic elements is $\pi/4$ which has been shown to be sufficient for the convergence of the results for M2PFC model [31]. As an example, the constructed two-phase FCC-liquid structure of Ni is shown in Fig. 2 where the normal direction is [110] (only the right-half section near the interface is shown).

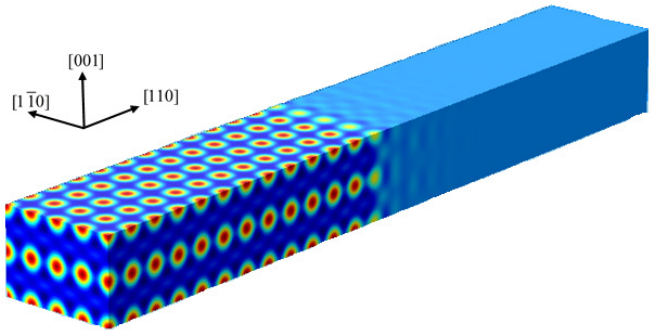

Fig. 2. The schematic of the coexisting two-phase FCC-liquid structure for Ni.

The FCC-liquid interface free energy in dimensional units is calculated using

$$\gamma = \frac{\lambda^2 q_0^{13}}{g\Omega} \int \{ f - (f_s \frac{\psi - \psi_l}{\psi_s - \psi_l} - f_l \frac{\psi - \psi_s}{\psi_s - \psi_l}) \} d\boldsymbol{r}, \tag{30}$$

where Ω is the FCC-liquid interface area. For illustration, the free energy density pattern the case of Al where the normal direction is [110] is depicted at Fig. 3.

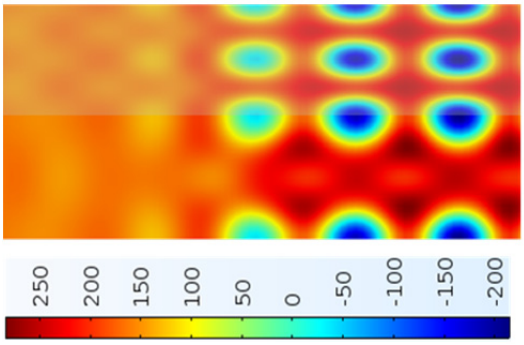

Figure 3. Free energy density (mJ/m^2) pattern at the {110} interface of two-phase FCC (right)-liquid (left) coexisting for Al.

The calculated FCC-liquid interface free energies for Ni and Al are reported in Table 6 along with the anisotropy parameter $\varepsilon_1 = (\gamma_{100} - \gamma_{110})/2\gamma_0$, where γ_0 is the average FCC-liquid interface free energy. The results show that the present PFC model slightly underestimates the interface free energies while predicts the anisotropy parameter in agreement with the experiments. It is worth mentioning that most of the previous MD works [33, 35] overestimated the interface free energy (with similar margin of errors). In the present model, R_1 parameter can be used to recover the exact interface free energies (rather than fitting to elastic constants) if one is interested in recovering the exact experimental interface free energies. As a final note we should mention that we used the $R_1 = -0.004$ that was determined for Ni to develop the model parameters for Al. It is possible to modify the parameters for Al in order to reduce the error in calculating the solid-liquid interface free energy of Al. Nevertheless, PFC modeling similar to any other computational model has certain number of model parameters that can be used to fit for a certain number of properties. The number of "unfitted" properties and their agreements with their experimental counterparts determine the predictive capability of the model. For the case of M2PFC model, interface free energies are the prediction of model and the amount of errors are reasonable comparing to the discrepancies in the calculations of other predictive computational models; e.g. MD calculations [33, 35]. Alternatively, extra parameters [36] or even extra terms [37] can be added into the free energy of the model in order to exactly fit to the interface free

energy; however, a careful attention must be devoted to not compromise the advantageous features of the model.

Table 6. Comparison of the PFC-calculated FCC-liquid interface free energy ($\gamma_{100}, \gamma_{110},$ and γ_0) and anisotropy parameter ($\varepsilon_1 = (\gamma_{100} - \gamma_{110}) / 2\gamma_0$) for Ni and Al with the available experimental data in literature.

Element	Method	γ_{100} (mJ/m^2)	γ_{110} (mJ/m^2)	γ_0 (mJ/m^2)	ε_1 (%)
Ni	PFC[a]	208.1	201.5	204.8	1.6
	Exp.	--	--	255[b], 300[c]	--
	MD	224[d]-	331[d]	310[d]-331.8[e]	1.2[d] -1.4[f]
Al	PFC[a]	73.4	71.2	72.3	1.5
	Exp.	--	--	93[b],108[c]	0.97[g],1.7[h]
	MD	131[i]	172[i]	149[i]-172.6 [e]	13.8[i]

[a] Present calculations.
[b] Homogeneous nucleation experiment [38].
[c] Maximum supercooling experiment [39].
[d] EAM-MD calculations [40].
[e] MEAM-MD calculations [41]
[f] EAM-MD calculations [42].
[g] Experimental measurement for Al-Cu [43].
[h] Experimental measurement for Al-Si [44].
[i] EAM-MD calculations [45].

4. CONCLUSIONS

It was shown that M2PFC model, which is a two-mode PFC model, can be directly derived from classical density functional theory. M2PFC was applied to FCC metals (Ni and Al as case studies). The model contains two independent parameters (ε and R_1) which were determined using an iterative procedure. Parameter ε was used to determine FCC-liquid coexisting densities, while parameter R_1 was used to calculate the solid elastic constants at the melting point. It was shown that the calculated elastic constants have been significantly improved comparing to the results of the previous two-mode PFC model for Ni. As a test for the quantitative capability of the model, the solid-liquid interface free energy and anisotropy of Ni

and Al were calculated. The calculated interface free energies were slightly lower than the experimental counterparts (the error margins are similar to MD overestimations of interface free energies). The anisotropy parameter of solid-liquid interface free energy for the model was in agreement with the experiments. The presented parameters for M2PFC in this work can be used in atomistic simulations of solidification and relevant phenomena for Ni and Al. In addition, the procedure presented here can be used to develop PFC model parameters for other FCC materials.

Acknowledgments

The authors are grateful for computer time allocation provided by the Extreme Science and Engineering Discovery Environment (XSEDE). M. Asle Zaeem would like to acknowledge the funding support from the National Science Foundation under Grant No. NSF-CMMI 1537170.

References

[1] M.S. Daw, M.I. Baskes, Physical Review B, 29 (1984) 6443.
[2] M. Baskes, Physical Review B, 46 (1992) 2727.
[3] H. Van Swygenhoven, A. Caro, D. Farkas, Materials Science and Engineering: A, 309 (2001) 440-444.
[4] V. Yamakov, D. Wolf, S.R. Phillpot, A.K. Mukherjee, H. Gleiter, Nature materials, 1 (2002) 45-49.
[5] E. Asadi, M.A. Zaeem, A. Moitra, M.A. Tschopp, Journal of Physics: Condensed Matter, 26 (2014) 115404.
[6] M. Asle Zaeem, H. El Kadiri, P. Wang, M. Horstemeyer, Computational Materials Science, 50 (2011) 2488-2492.
[7] M. Asle Zaeem, H. Yin, S. Felicelli, Applied Mathematical Modeling, 37 (2013) 3495–3503.
[8] M. Asle Zaeem, H. Yin, S.D. Felicelli, Materials Science & Technology, 28 (2012) 137-146.
[9] E. Asadi, M. Asle Zaeem, JOM, 67 (2015) 186-201.
[10] K. Elder, M. Katakowski, M. Haataja, M. Grant, Physical Review Letters, 88 (2002) 245701.
[11] K.R. Elder, M. Grant, Physical Review E, 70 (2004) 051605.
[12] H. Emmerich, H. Löwen, R. Wittkowski, T. Gruhn, G.I. Tóth, G. Tegze, L. Gránásy, Advances in Physics, 61 (2012) 665-743.
[13] H. Humadi, N. Ofori-Opoku, N. Provatas, J.J. Hoyt, JOM, 65 (2013) 1103-1110.
[14] S. van Teeffelen, R. Backofen, A. Voigt, H. Löwen, Physical Review E, 79 (2009) 051404.
[15] L. Gránásy, F. Podmaniczky, G.I. Tóth, G. Tegze, T. Pusztai, Chemical Society Reviews, 43 (2014) 2159-2173.
[16] N. Pisutha-Arnond, V. Chan, K. Elder, K. Thornton, Physical Review B, 87 (2013) 014103.
[17] J. Berry, K. Elder, M. Grant, Physical Review B, 77 (2008) 224114.
[18] J. Mellenthin, A. Karma, M. Plapp, Physical Review B, 78 (2008) 184110.
[19] K. Elder, K. Thornton, J. Hoyt, Philosophical Magazine, 91 (2011) 151-164.
[20] E. Asadi, M. Asle Zaeem, Computational Materials Science, 105 (2015) 110-113.
[21] E. Asadi, M. Asle Zaeem, M.I. Baskes, JOM, 66 (2014) 429-436.

[22] E. Asadi, M. Asle Zaeem, S. Nouranian, M.I. Baskes, Physical Review B, 91 (2015) 024105.
[23] A. Jaatinen, C. Achim, K. Elder, T. Ala-Nissila, Physical review E, 80 (2009) 031602.
[24] K.-A. Wu, A. Adland, A. Karma, Physical Review E, 81 (2010) 061601.
[25] J. Swift, P. Hohenberg, Physical Review A, 15 (1977) 319-328.
[26] R. Lifshitz, D.M. Petrich, Physical review letters, 79 (1997) 1261.
[27] A. Emdadi, M. Asle Zaeem, E. Asadi, Computational Materials Science, 123 (2016) 139-147.
[28] Y.J. Gao, W.Q. Zhou, Y. Liu, C.G. Huang, Q.H. Lu, Advanced Materials Research, 785 (2013) 512-516.
[29] A. Adland, Y. Xu, A. Karma, Physical review letters, 110 (2013) 265504.
[30] T. Ramakrishnan, M. Yussouff, Physical Review B, 19 (1979) 2775.
[31] E. Asadi, M. Asle Zaeem, Computational Materials Science, 105 (2015) 101-109.
[32] Y. Waseda, The structure of non-crystalline materials: liquids and amorphous solids, McGraw-Hill New York, 1980.
[33] E. Asadi, M. Asle Zaeem, S. Nouranian, M.I. Baskes, Acta Materialia, 86 (2015) 169-181.
[34] E. Asadi, M.A. Zaeem, Computational Materials Science, 105 (2015) 101-109.
[35] E. Asadi, M. Asle Zaeem, Acta Materialia, 107 (2016) 337-344.
[36] A. Nourian-Avval, E. Asadi, Comutational Materials Science, Under Revision (2016).
[37] C. Guo, J. Wang, Z. Wang, J. Li, Y. Guo, Y. Huang, Soft matter, 12 (2016) 4666-4673.
[38] D. Turnbull, Journal of Applied Physics, 21 (1950) 1022-1028.
[39] K. Kelton, Solid state physics, 45 (1991) 75-177.
[40] M. Asta, J. Hoyt, A. Karma, Physical Review B, 66 (2002) 100101.
[41] E. Asadi, M.A. Zaeem, S. Nouranian, M.I. Baskes, Acta Materialia, 86 (2015) 169-181.
[42] J. Hoyt, M. Asta, A. Karma, Materials Science and Engineering: R: Reports, 41 (2003) 121-163.
[43] S. Liu, R. Napolitano, R. Trivedi, Acta Materialia, 49 (2001) 4271-4276.
[44] R. Napolitano, S. Liu, R. Trivedi, Interface Science, 10 (2002) 217-232.
[45] J.R. Morris, Physical Review B, 66 (2002) 144104.